Optical Materials 36 (2014) 879–884

Contents lists available at ScienceDirect

Optical Materials

journal homepage: www.elsevier.com/locate/optmat

Structural and photoluminescence properties of Mg substituted ZnO nanoparticles

A.N. Mallika *, A. Ramachandra Reddy, K. Sowri Babu, Ch. Sujatha, K. Venugopal Reddy

Department of Physics, Materials Science Laboratory, National Institute of Technology, Warangal 506 004, Andhra Pradesh, India

ARTICLE INFO

Article history:
Received 23 July 2013
Received in revised form 21 November 2013
Accepted 8 December 2013
Available online 7 January 2014

Keywords:
Mg substituted ZnO nanoparticles
Sol–gel method
Structural properties
Photoluminescence

ABSTRACT

This paper reports on structural and optical properties of Mg doped ZnO nanoparticles prepared through sol–gel method using polyvinyl alcohol as chelating agent. X-ray diffractometer (XRD), Field Emission Scanning Electron Microscope (FE-SEM), UV–Vis (UV–Vis), Fourier Transform Infrared (FTIR) and Photoluminescence (PL) spectrophotometers were employed to study the structural and optical properties. XRD and FE-SEM results demonstrated that particle size of ZnO decreased with increase in Mg concentrations. It was observed that the absorption spectrum of ZnO blue shifted as the Mg concentration enhanced from 1 mol.% to 5 mol.%, presumably due to reduction in particle size. It was found that MgO secondary phase was not formed even above the solid solubility limit of Mg in ZnO. ZnO nanoparticles exhibited an intense and strong UV emission peak at 396 nm and this peak is attributed to the electron transition from the localized level slightly below conduction band to the valence band. The position of this emission peak remained same for all concentrations of Mg in ZnO.

1. Introduction

ZnO is one of the II–VI group n-type semiconductors, which is having a wurtzite structure with hexagonal unit cell (P63mc) [1]. The large band gap and high exciton binding energy of ZnO (3.37 eV and 60 meV) ensures stable exciton emission even at room temperature. The chemical and thermal stability of ZnO makes it, as a potential candidate for light emission applications [2]. Moreover, ZnO is a cheap, nontoxic, bio-safe material [3]. Because of the above advantages, it has applications in the areas of transparent high power electronics, surface acoustic wave devices, piezo-electric transducers, gas-sensing, and as a window material for display, spin-electronics, non-linear optical devices and solar cells etc. [4]. Apart from the above, ZnO is an important luminescent material in short wave length optoelectronic devices, such as ultraviolet light emitting diodes (LEDs) and Laser diodes (LD's) due to its large excitation binding energy [5]. A variety of ZnO nanostructures such as nanodots, nanorods, nanoleaves, nanoflowers, nanobelts/ribbons, nanowires and tetrapods have been reported which give rise to interesting optical properties [6]. The properties of ZnO nanoparticles strongly depend on its crystallite size and morphology which in turn rely on the synthesis methods [7]. ZnO nanoparticles can be prepared mainly through vapour, the solution and the solid phase methods [8]. Various approaches have been developed for the preparation of ZnO nanopowders such as co-precipitation, hydrothermal, Ultrasonic, spray pyrolysis and sol–gel methods. Among them, sol–gel method is mostly preferable because of its simplicity, ease of controllability of compositions, repeatability and being less expensive. ZnO, at nanoscales exhibit novel physical properties which are substantially different from their bulk counterparts. To enhance the electrical and optical properties of ZnO, doping with suitable transition elements has been preferred [9]. Djurisic reported that, ZnO mainly can be doped in four ways: doping with (1) donor impurities to achieve n-type conductivity, (2) acceptor impurities to achieve p-type conductivity, (3) rare-earth elements to achieve desired optical properties and (4) transition metals to achieve desired magnetic properties. Doping of ZnO with different donors broadened the UV emission peak and also shifted according to the type of doping element [10]. The doping of Mg in ZnO is preferred due to the following reasons; (i) The ionic radius of Mg^{2+} (0.57 Å) is comparable to the ionic radius of Zn^{2+} (0.60 Å). (ii) Doping of Mg in ZnO permits the band gap to be tailored and also Mg doped Zn leaves the lattice constants almost invariant due to the high solid solubility of MgO in ZnO. It was observed that substitution of Mg in ZnO resulted in enhancement of the UV luminescence intensity as well as its band gap [11]. But, the thermodynamic solubility limit of MgO in ZnO is less than 4 mol.% as suggested by the phase diagram of MgO–ZnO binary system [12]. There are several reports on the luminescence properties of $Mg_xZn_{1-x}O$ for

* Corresponding author. Tel.: +91 870 2462593; fax: +91 870 2459547.
E-mail addresses: mallika.nitw@gmail.com, a.n.mallika.phy@gmail.com (A.N. Mallika).

0925-3467/$ - see front matter © 2013 Elsevier B.V. All rights reserved.
http://dx.doi.org/10.1016/j.optmat.2013.12.015

different x values. A better thermal stability of Mg in $Mg_xZn_{1-x}O$ can be obtained for $x \leqslant 0.15$ [13]. Moreover, it was reported that incorporation of Mg into ZnO tends to decrease the interstitial oxygen vacancies and electron density [14]. So, Mg doping will have considerable influence on the optical properties of ZnO and it paves the way to obtain tunable electrical and optical properties.

In this paper, the structural and optical properties of Mg doped ZnO nanoparticles prepared through sol–gel method were investigated. $Mg_xZn_{1-x}O$ samples were prepared with different 'x' values ranging from 0.01 to 0.05 mol%. The particle size reduced from 35 nm to 28 nm with Mg doping. A blue shift of about 10 nm in absorption peak was observed with Mg doping from $x = 0.01$ to 0.05. The intensity of UV emission peak positioned at 396 nm was decreased with increase of Mg concentration but its position remained unchanged.

2.1. Experimental details

ZnO nanoparticles were prepared through sol–gel method described elsewhere [15]. Zinc nitrate hexahydrate (Zn (NO3)2·6H2O), Magnesium nitrate hexahydrate (Mg (NO3)2·6H2O) were used as starting chemicals for the synthesis of $Mg_xZn_{1-x}O$. All the chemical ingredients are AR grade of HI-Media and were weighed in stoichiometric proportions for getting 2 g of final product and were dissolved in 30 ml of deionised water. One of these sets left undoped, whereas in the remaining set, magnesium nitrate was added to obtain the sol containing $x = 0.01, 0.02, 0.03, 0.04$, and 0.05 in $Mg_xZn_{1-x}O$, and were named here after as undoped, Mg1, Mg2, Mg3, Mg4 and Mg5 respectively. These metal nitrates were stirred continuously with the help of magnetic stirrer in order to get a homogeneous transparent solution. The PVA to metal ions ratio was maintained as 3:1 for all sets of samples. The weighed PVA (6 g) was added slowly to 60 ml of deionised water and stirred continuously for 3–4 h in order to get homogeneous milk white solution. Then metal nitrate solution was added drop by drop to the aqueous PVA at 70 °C and stirred thoroughly until a viscous gel is obtained. Then the gel was kept in an oven at 150 °C in order to get a dried powder. Then samples were annealed at 600 °C at a rate of 2 °C /min to obtain $Mg_xZn_{1-x}O$ with different x values.

2.2. Characterization

The phase identification and crystallite sizes were determined using X-ray diffraction (XRD) patterns recorded on INEL XRG 3000 powder diffractometer equipped with Co Kα radiation ($\lambda = 1.7889$ Å) in terms of 2θ ranging from 20° to 120°. The morphology and the grain size distribution of Mg doped ZnO nanoparticles were investigated using FE-SEM (Model: Carl Zeiss Ultra 55) operating at an accelerating voltage of 17 KV with a working distance (WD) of 8.5 mm. The elemental analysis of the annealed samples was carried out using energy dispersive X-ray spectroscopy (EDAX) attached to FE-SEM. Formation of ZnO was confirmed from FTIR spectrum (Model: PerkinElmer Spectrum-100) recorded in the wave number region 4000–400 cm^{-1}. Optical absorption of the samples was recorded using (Model: Thermo Scientific, evolution 600 UV–Vis) UV–Vis spectrophotometer in the wave length region of 250–450 nm. The PL measurements were performed on Jobin Yuon spectrofluorometer (Model: Fluorolog-Fl3-11) with wavelength resolution of 0.2 nm at room temperature. The Xenon arc lamp of 450 W was used as the excitation light source to record the emission spectra of the samples.

Table 1
Crystallite size from Debye-Scherrer's, W-H plot and corresponding strain.

Sample name	Stain (ε) × 10^{-4}	Crystallite size (nm)	
		W–H plot	Scherrer's formula
Pure	1.494	40.88	35
Mg1	1.49902	40.8	34
Mg2	1.14142	43.9	36.8
Mg3	1.52837	47	36.2
Mg4	1.69308	40.17	34
Mg5	1.9111	33.5	28

3. Results and discussions

3.1. XRD analysis

The crystal structures of the samples were investigated by analysing the XRD data. The X-Ray diffraction patterns of Mg doped ZnO nanopartices shown in Fig. 1. The XRD peaks were indexed by comparing the observed data with the standard JCPDS No. 03-0888. The peaks at $2\theta = 37.123°$, 40.246°, 42.284°, 55.850°, 67.029°, 74.369°, 80.809°, and 82.251° correspond to (100), (002), (101), (102), (110), (103), (112), and (201) diffraction planes of ZnO hexagonal structure [16]. No other secondary phase, such as MgO was observed indicating the pure ZnO phase of the sample. Mg substitution did not alter the wurtzite structure of ZnO which may be attributed to the small amounts of Mg concentrations in the sample. Moreover, cubic MgO phase was not detected when the Mg concentration is less than 0.15 in $Mg_xZn_{1-x}O$ [11]. It represents that Mg successfully replaced the Zn lattice site rather than the interstitial one. The average particle size (d_{avg}) of the prepared samples was estimated from the width of reflection peaks in the XRD spectrum using the Debye Scherrer's equation [17].

$$d_{xrd} = \frac{0.9\lambda}{\beta \cos\theta} \tag{1}$$

where, $\beta = \sqrt{(\beta^2_{FWHM} - \beta^2_o)}$ is the peak broadening after removing the instrumental broadening, β_{FWHM} is the full width at half maximum and β_o is the correction factor (0.007 radians). The crystallite size values were calculated using Scherrer's formula and are shown in Table 1. It was observed that the crystallite size decreased with increase of Mg concentration. It indicates that smaller particles can be obtained at higher concentrations of Mg. During the doping

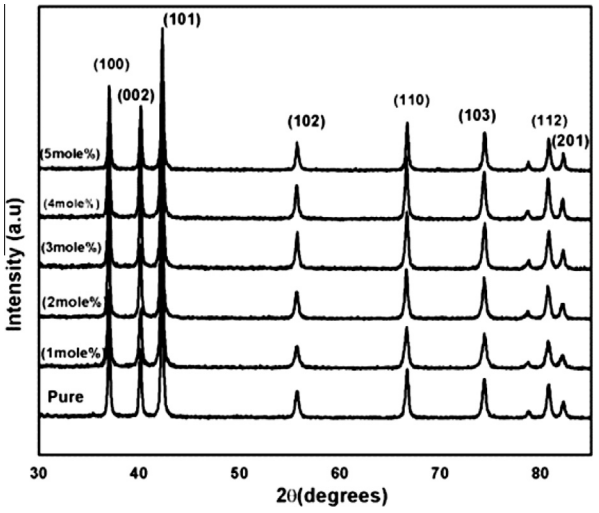

Fig. 1. The X-ray diffraction pattern of the ZnO and Mg doped ZnO samples.

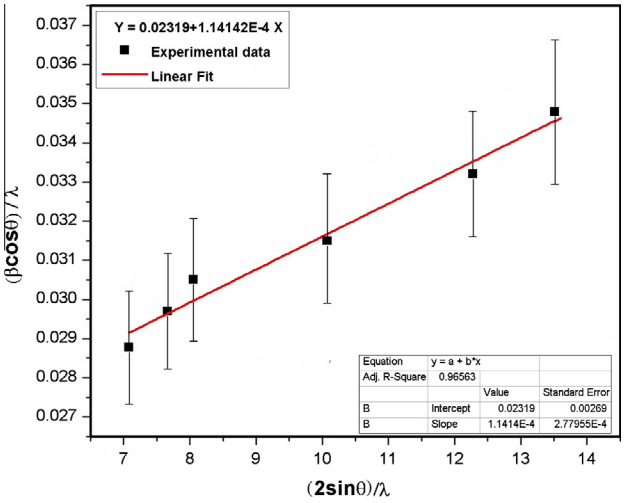

Fig. 2. Williamson–Hall plot of one of the Mg substituted sample.

process, Mg atoms may be located in or near the boundary of ZnO nanoparticles, resulting in decrease of diffusion rate thereby preventing growth of nanoparticles. Hence there is a decrease in ZnO crystallite size with Mg doping [18]. This decrease in the particle size with increasing levels of Mg doping has influence on the absorption spectra [19]. Apart from the crystallite size, lattice strain also contributes to the broadening of the XRD peaks. The effect of lattice strain on peak broadening of the diffraction peaks can be estimated by the Williamson–Hall and the size strain plot (SSP) method [20]. In this study, the strain broadening of the diffraction peaks was evaluated using W–H analysis. It clearly differentiates between size induced and strain induced peak broadenings by considering the peak width as a function of 2θ. The average crystallite size and strain in the nanoparticles were calculated from the spectral line shape using Williamson–Hall (W–H) plot based on the following equation [21] (see Fig. 1).

$$\frac{\beta\cos\theta}{\lambda} = \frac{0.9}{d} + \frac{4\varepsilon\sin\theta}{\lambda} \tag{2}$$

where β is the full width at half maximum, ε is the lattice strain and θ is the Bragg angle, d is the average particle size and λ is the wavelength of the X-rays. The strain was calculated from the slope of the linear fit and the y-intercept gives the inverse particle size from Fig. 2. The estimated strain and crystallite size from W–H plot was tabulated. It was observed from Table 1, that crystallite size estimated using W–H plots followed the same trend as observed in Debye Scherrer's formula. The strain calculated was increased with Mg substitution. Muthukumaran et al. reported that, decrease in strain caused the increase of crystal size and reduction in the peak broadening whereas increase of strain caused reduction of crystal size and increase of peak broadening [22]. The effect of stain on optical properties is discussed in detail in the following discussion.

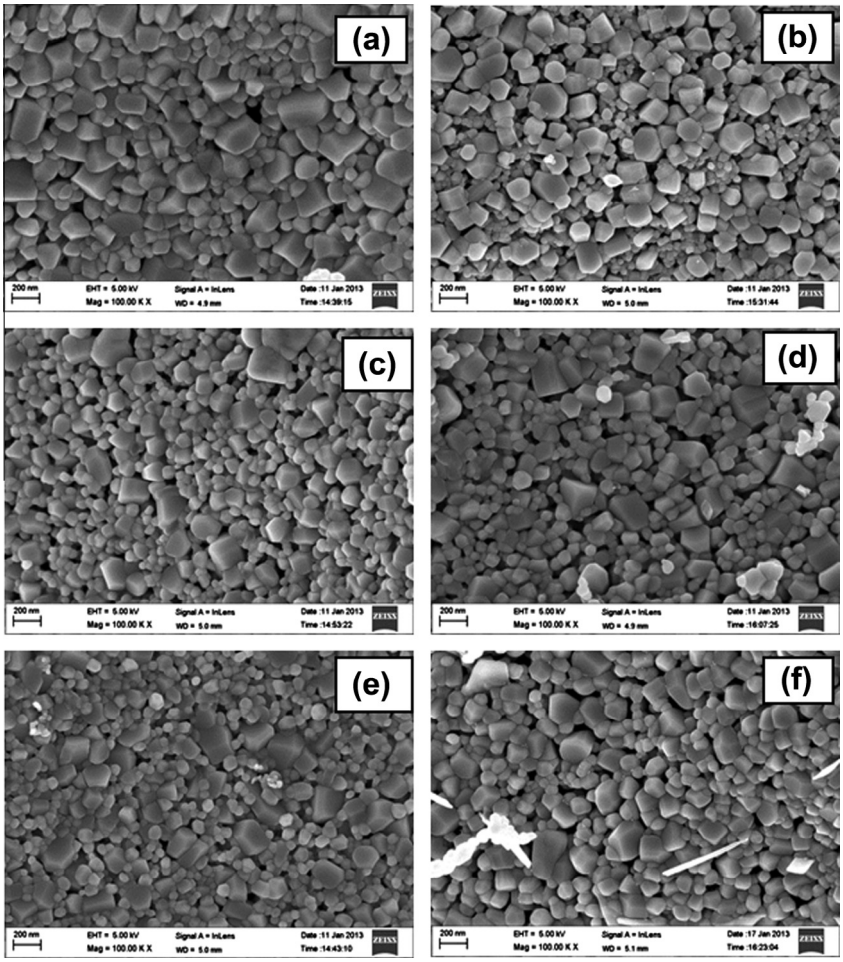

Fig. 3. FE-SEM micrographs of $Mg_xZn_{1-x}O$ (a) un doped ZnO, (b) Mg1, (c) Mg2, (d) Mg3, (e) Mg4 and (f) Mg5.

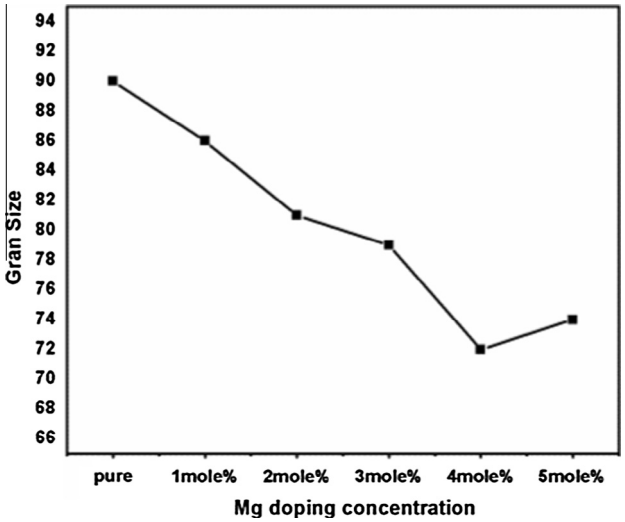

Fig. 4. The grain size vs the Mg concentration.

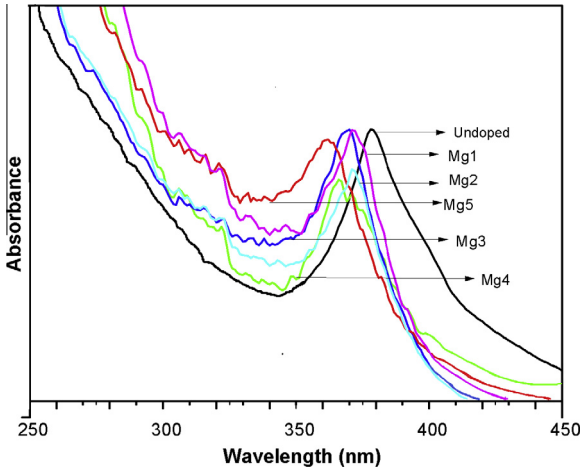

Fig. 6. Absorption spectrum of undoped and doped ZnO samples.

3.2. SEM

In general, the morphology of the samples was analysed by FE-SEM to examine diameter, length, shape, and density of the nanostructure [23]. The FE-SEM pictures of ZnO and Mg doped ZnO are shown in Fig. 3. The microstructure of the samples showed polyhedral shaped grains of different sizes. The particle size values for pristine ZnO and Mg doped ZnO nanoparticles were in the range of 90 nm, 86 nm, 81 nm, 79 nm, 72 nm, and 74 nm for undoped, Mg1, Mg2, Mg3, Mg4 and Mg5 respectively. These results indicate the particle size decreased gradually with increase of Mg concentration which is in good agreement with the particle sizes obtained from XRD. The plot drawn between grain sizes and Mg concentrations showed that there is a decrease in grain size with increase of Mg concentration as shown in Fig. 4. The EDAX analysis of the samples confirmed the presence of Mg in the samples as shown in Fig. 5. The other elements such as gold and copper visible in EDAX spectra of samples are due to coatings made for better conductivity and copper grid was used to mount the samples.

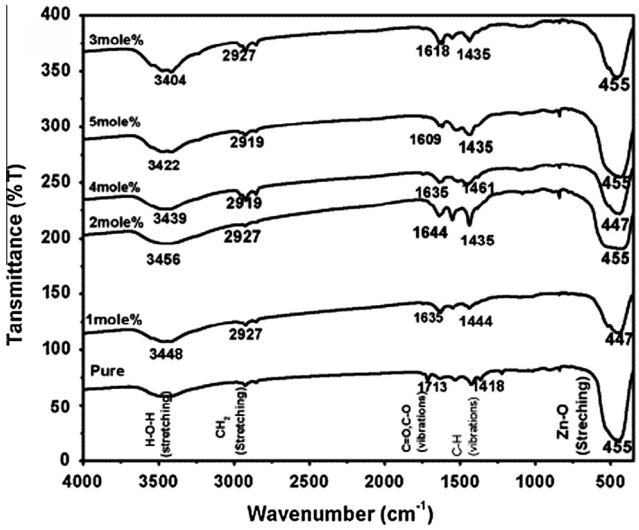

Fig. 7. FTIR spectra of $Mg_xZn_{1-x}O$ (x = 0, 0.01, 0.02, 0.03, 0.04 and 0.05).

3.3. UV–Vis Analysis

The UV–Vis absorption spectra of ZnO and the $Mg_xZn_{1-x}O$ nanoparticles were taken by dispersing them in ethanol is shown in Fig. 6. The absorption depends on several factors such as band gap, Oxygen deficiency, size and structure of the nanoparticles, surface roughness and impurity centres [9]. ZnO nanoparticles exhibited an absorption peak centred at 377 nm which is due to fundamental absorption of excitons. This absorption peak was blue

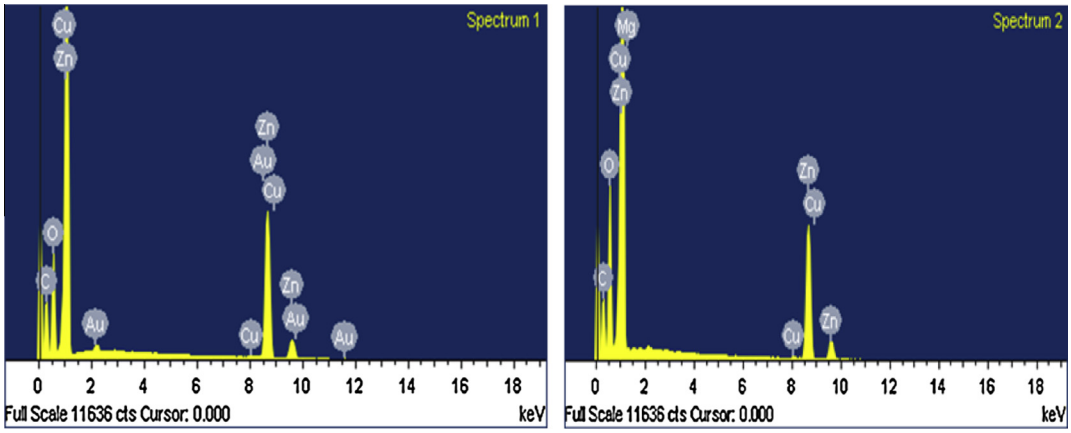

Fig. 5. EDAX pictures of ZnO and Mg doped ZnO.

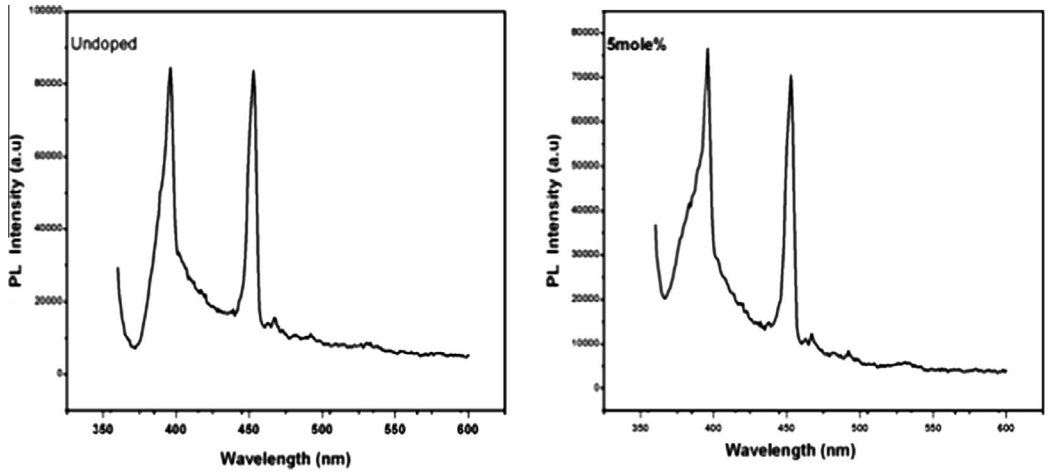

Fig. 8. PL spectrum of the undoped and Mg doped ZnO at 5 Mg.

shifted from 377 nm to 362 nm with increase in Mg doping due to the quantum confinement effects of ZnO nanoparticles. Using effective mass approximation, the energy corresponding to the exciton absorption peak has been converted in terms of particle size [24]

$$E = E_g + h^2\pi^2\left(\frac{1}{m_e} + \frac{1}{m_h}\right) - \left(\frac{1.8e^2}{4\pi\varepsilon'\varepsilon_o R}\right) + Smallerterm \quad (3)$$

where E is the band gap of the synthesised particle, E_g is the bulk energy of ZnO (3.37 eV), R is the radius of the particle, m_e is the effective mass of the electron ($0.28mo$), m_h is the effective mass of the hole ($0.49mo$), ε' is the dielectric constant of the material (9.1), ε_o is the permittivity of the free space, h is the Planck's constant. The obtained values of the particle radius from the mass approximation for undoped, Mg1, Mg2, Mg3, Mg4 and Mg5 are 4.05 nm, 3.344 nm, 3.244 nm, 3.06 nm, 2.854 nm, and 2.99 nm respectively.

3.4. FTIR analysis

The Infrared spectra of Mg doped ZnO nanoparticles recorded in the region of 4000–400 cm−1 are shown in Fig. 7. The wide intense absorption peaks positioned at 3417–3479 cm^{-1} corresponds to OH-group stretching vibrations due to the bound H_2O on the surface of the nanocrystalline powder sample. The FTIR bands around 2900 cm−1 belongs to CH2 stretching vibration, 1609 cm−1 to 1713 cm−1 correspond to asymmetric and symmetric stretching vibrations of carboxyl group (C=O). One large band located at 455 to 447 cm−1 can be attributed to Zn—O stretching in the ZnO lattice [16,23]. This study confirmed that the organic complexes and residues in ZnO are eliminated completely at the annealing temperature of 600 °C. Thus FTIR spectra corroborated the formation of ZnO wurtzite structure. By careful observation of the spectra, it is clear that there is a slight broadening of Zn—O stretching peak at various increased Mg concentrations. This may be due to some of the substituted Mg ions at Zn sites. Thus from FTIR spectrum, it can be confirmed that the Mg successfully replaced the Zn sites.

3.5. Photoluminescence

The photoluminescence spectrum provides information on the optically active defects and relaxation pathways of the excited states [25]. In most of the cases, the photoluminescence (PL) of the ZnO nanoparticles have been showed two components. One is the typical exciton emission, that is, photo generated electrons recombine with the holes at the valence band emitting UV light. The other is the defect based emission which is generally located in the visible region of the PL spectrum and its exact mechanism is not fully understood yet [20]. Fig. 8 Shows the PL spectra of undoped ZnO and Mg doped ZnO nanoparticles recorded with an excitation wavelength of 353 nm. The PL spectrum of ZnO showed a sharp peak positioned at 395 nm. This sharp emission peak observed at 396 nm is due to the electron transition from the localized level slightly below the conduction band to the valence band [15]. Another sharp peak at 453 nm is due to the substrate which has been used to hold the sample [26]. Srikant and Clarke et al. assigned a peak at around 396 nm to a shallow donor, and the nature of the shallow donor might be the complex defect of Zn_i [27]. Generally observed green emission is not observed in this study. The position of the 396 nm UV emission peak did not change with Mg concentration. This absence of the shift infers that 396 nm peak is originated from defect level. The blue shift observed in absorption spectrum was not reflected in emission spectrum. This may be due to the fact that the emission peak at 396 nm is originated due to the transition from defect level to the valence band. It is observed from Fig. 8 that PL spectrum of Mg5 sample showed a kink at 383 nm. It is reported that the near band edge emission from these ZnO nanoparticles is positioned at 384 nm [15]. So, the emission peak at 383 nm is the near band edge emission. It indicates that near band edge emission has been induced by the Mg doping. The strong UV emission intensity at room temperature should be attributed to high purity ZnO nanoparticles with perfect crystallinity [28]. The broadening of the PL spectrum with Mg doping may be due to the strain developed and also due to increase in 384 nm band edge emission. The FWHM values of UV emission for undoped ZnO and Mg1, Mg2, Mg3, Mg4 and Mg5 samples are 11 nm, 11.6 nm, 13 nm, 14.3 nm, 14.26 nm and 13.3 nm respectively. FWHM of the UV emission peak increased with an increase of Mg concentration. This reveals the narrow size distribution of the nanoparticles [29]. Further, intensity of UV emission peak decreased with increase of Mg concentration. This reduction is due to decrease in crystallinity with increase of Mg concentration.

4. Conclusions

ZnO nanoparticles were successfully synthesised using PVA as chelating agent. The structural and optical properties of undoped and Mg doped ZnO nanoparticles were studied. The maximum crystallite size obtained from XRD is less than 50 nm and the

XRD pattern confirmed the polycrystalline hexagonal wurtzite structure of ZnO. Mg substitution increased the strain in the lattice. The grain size estimated from FE-SEM studies decreased with increasing Mg substitution. The evaluated particle sizes of the ZnO and Mg doped ZnO samples from UV–Vis as well as XRD exhibited the same trend. With the increase in Mg concentrations, there was a blue shift observed in the absorption peaks, indicating decrease in the particle size. It can be concluded that even with small amount of substitution of Mg in ZnO (5%); it produced a microstrain which changed the absorption as well as the near band emission. The PL spectra of the samples showed a strong UV emission band, located at 396 nm which is because of the transition of electron just below the conduction band to valence band but it is not a near band edge emission.

Acknowledgements

Authors wish to thank Prof. S.P. Tiwari, Dean, School of Physics, University of Hyderabad (UOH) for providing XRD and FE-SEM facility. The authors are also thankful to the Department of Chemistry National Institute of Technology Warangal, for providing FTIR, and UV–Vis measurements.

References

[1] N. Rajeswari Yogamalar, A. Chandra Bose, Absorption-emission of hydrothermally grown Al: ZnO nanostructures, J. Alloys Compd. 509 (2011) 8493–8500.
[2] S. Singh, P. Thiyagarajan, K. Mohan Kant1, D. Anita, S. Thirupathiah, N. Rama, B. Tiwari, M. Kottaisamy, M.S. Ramachandra, Structure, microstructure and physical properties of ZnO based materials in various forms: bulk, thin film and nano, J. Phys. D: Appl. Phys. 40 (2007) 6312–6327.
[3] Gyu-Chul Yi, C. Wang, Won Il Park, ZnO nanorods: synthesis, characterization and applications, Semicond. Sci. Technol. 20 (2005) S22–S34.
[4] S.J. Pearton, D.P. Norton, K. Ip, Y.W. Heo, T. Steiner, Recent progress in processing and properties of ZnO, Prog. Mater Sci. 50 (2005) 293–340.
[5] K. Balchandra Kumar, P. Raji, Synthesis and characterization of nanoZinc oxide by sol gel spin coating, Recent Res. Sci. Technol. 3 (3) (2011) 48–52.
[6] M. Willander, Q.X. Zhao, Q.H. Hu, P. Klason, V. Kuzmin, S.M. Al-Hilli, O. Nur, Y.E. Lozovik, Fundamentals and properties of zinc oxide nanostructures: optical and sensing applications, Superlattices Microstruct. 43 (2008) 352–361.
[7] D.L. Golic, G. Brankovic, M.P. Nesic, K. Vojisaljevic, A. Recnik, N. Daneu, S. Bernik, M. Scepanovic, D. Poleti, Z. Brankovic, Structural charecterization of self-assembled ZnO nanoparticles obtained by the sol–gel method from Zn $(CH_3COO)_2$, Nanotechnology 22 (2011) 395603 (9pp).
[8] Davood. Raoufi, Synthesis and microstructural properties of ZnO nanoparticles prepared by precipitation method, Renew. Energy 50 (2013) 932–937.
[9] Imran Khan, Shakeel Khan, Razia Nongjai, Hilal Ahmed, Wasi Khan, Structural and optical properties of Zr doped ZnO nanoparticles, Opt. Mater. 35 (2013) 1189–1193.
[10] Aleksandra B. Djurisic, Y.H. Leung, Optical properties of ZnO nanostructures, Small 2 (8–9) (2006) 944–961.
[11] Junlin Li, H. Zhuang, Jie Wang, Peng Xu, Synthesis, characterization, and optical properties of Mg-doped zinc oxide single-crystal microprisms, Phys. Status Solidi A 208 (1) (2011) 136–139. doi: 10.1002/pssa.201026448.
[12] E.R. Segnit, A.E. Holland, The system MgO–ZnO–SiO_2, J. Am. Ceram. Soc. 48 (1965) 412.
[13] A. Dev, S. Chakrabarti, S. Kar, S. Chaudhuri, Optical properties of Mg0.05Zn0.95O/SiO2 nanocomposite films prepared by sol–gel technique, J. Nanopart. Res. 7 (2005) 195–201.
[14] Chien-Yie Tsay, Min-Chi Wang, Shin-Chuan Chiang, Effects of Mg additions on microstructure and optical properties of sol–gel derived ZnO thin films, Mater Trans. 49 (2008) 1186–1191.
[15] K. Sowri Babu, A. Ramachandra Reddy, Ch. Sujatha, K. Venugopal Reddy, Optimization of UV emission intensity of ZnO nanoparticles by changing the excitation wavelength, Mater. Lett. 99 (2013) 97–100.
[16] Guang-Hui Ning, Xiao-Peng Zhao, Jia Li, Structure and optical properties of $Mg_xZn_{1-x}O$ nanoparticles prepared by sol–gel method, Opt. Mater. 27 (2004) 1–5.
[17] B.D. Cullity, Elements of X-ray Diffractions, Addison-Wesley, Reading, MA, 1978. p. 102.
[18] M.Z. Nursyahadah, S.S. Nurul, Z. Azlan, M.T. Kumar, Effect of magnesium doping on structural and optical properties of ZnO nanoparticles synthesized by mechanochemical processing, AIP Conf. Proc. 1328 (2011) 211, http://dx.doi.org/10.1063/1.3573732.
[19] Y.S. Wang, P.J. Thomas, P. O'Brien, Optical properties of ZnO nanocrystals, J. Phys. Chem. B 110 (43) (2006).
[20] R. Yousefi, A.K. Zak, F.J. Sheini, Growth, X-ray peak broadening studies, and optical properties of Mg-doped ZnO nanoparticles, Mater. Sci. Semiconduct. Proc. 16 (2013) 771–777.
[21] K. Venkateswarlu, A. Chandra Bose, N. Rameshbabu, X-ray peak broadening studies of nanocrystalline hydroxyl apatite by Williamson–Hall analysis, Physica B 405 (2010) 4256–4261.
[22] S. Muthukumaran, R. Gopalakrishnan, Structural, optical, FTIR and photoluminescence properties of $ZnO_{0.96-x}Co_{0.04}Cu_xO$ ($x = 0.03$, 0.04 and0.05) nanopowders, Physica B 407 (2012) 3448–3456.
[23] K. Vijayalakshmi, K. Karthick, Influence of annealing on the Photoluminescence of nanocrystalline ZnO synthesized by microwave processing, Philos. Mag. Lett. 92 (12) (2012) 710–717.
[24] A.K. Singh, V. Viswanath, V.C. Janu, Synthesis, effect of capping agents, structural, optical and photoluminescence properties of ZnO nanoparticles, J. Lumin. 129 (2009) 874–878.
[25] C. Ravichandran, G. Srinivasan, C. Lenon, S. Sivanathan, J. Kumar, Influence of post-deposition annealing on the structural, optical and electrical properties of Li and Mg co-doped ZnO thin films deposited by sol–gel technique, Superlattices Microstruct. 49 (2011) 527–536.
[26] K. Sowri Babu, A. Ramachandra Reddy, Ch. Sujatha, K.V.G. Reddy, A.N. Mallika, Annealing effects on photoluminescence of ZnO nanoparticles, Mater. Lett. 110 (2013) 10–12.
[27] V. Srikant, D.R. Clarke, On the optical band gap of Zinc oxide, J. Appl. Phys. 83 (1998) 5447–5451.
[28] N.C. Das, S. Upreti, P.E. Sokol, Small angle neutron scattering and photoluminescence property of wet chemistry process synthesized ZnO nanoparticles, J. Exp. Nanosci. 5 (2010) 180–187.
[29] B. SrinivasaRao, B. RajeshKumar, V. RajagopalReddy, T. SubbaRao, Preparation and characterization of CdS nanoparticles by chemical co-precipitation technique, Chalcogenide Lett. 8 (2011) 177–185.